JACS
JOURNAL OF THE AMERICAN CHEMICAL SOCIETY
Article
pubs.acs.org/JACS

Enzymatic Single-Molecule Kinetic Isotope Effects

Christopher R. Pudney,[†,†] Richard S. K. Lane,[‡] Alistair J. Fielding,[‡] Steven W. Magennis,[‡] Sam Hay,[†] and Nigel S. Scrutton*[,†]

[†]Manchester Institute of Biotechnology and Faculty of Life Sciences, University of Manchester, 131 Princess Street, Manchester M1 7DN, U.K.

[‡]The Photon Science Institute and School of Chemistry, University of Manchester, Oxford Road, Manchester M13 9PL, U.K.

Supporting Information

ABSTRACT: Ensemble-based measurements of kinetic isotope effects (KIEs) have advanced physical understanding of enzyme-catalyzed reactions, but controversies remain. KIEs are used as reporters of rate-limiting H-transfer steps, quantum mechanical tunnelling, dynamics and multiple reactive states. Single molecule (SM) enzymatic KIEs could provide new information on the physical basis of enzyme catalysis. Here, single pair fluorescence energy transfer (spFRET) was used to measure SM enzymatic KIEs on the H-transfer catalyzed by the enzyme pentaerythritol tetranitrate reductase. We evaluated a range of methods for extracting the SM KIE from single molecule spFRET time traces. The SM KIE enabled separation of contributions from nonenzymatic protein and fluorophore processes and H-transfer reactions. Our work demonstrates SM KIE analysis as a new method for deconvolving reaction chemistry from intrinsic dynamics.

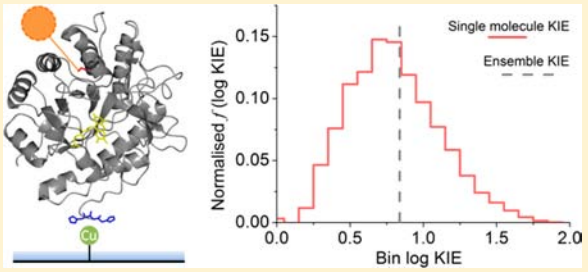

INTRODUCTION

Most enzyme-catalyzed reactions involve electron and hydrogen transfer. The kinetics of H-transfer reactions are sensitive to isotopic substitution and measurements of kinetic isotope effects (KIEs) are powerful probes of these reactions. KIEs are commonly used to probe chemical mechanisms that involve H-transfer, reporting specifically on the properties of the chemical (H-transfer) step. In ensemble enzyme turnover studies, KIE measurements have provided insight into transition state structures,[1−3] rate-limiting steps,[4,5] and reaction geometries within reaction series (e.g., a series of variant enzymes[6−9] or across different substrates,[10,11]), or through perturbation of active site structure induced by other changes (e.g., temperature[12−14] or hydrostatic pressure[15]). Here, we demonstrate the feasibility of measuring enzymatic KIEs for a hydride transfer reaction at the single-molecule (SM) level using single-pair fluorescence resonance energy transfer (spFRET). SM measurements provide an alternative kinetic probe of reaction dynamics, which complement more common (pre)steady-state measurements. SM spectroscopy (SMS) augments studies at the ensemble level. For example, SMS can identify alternative catalytic states that would otherwise be masked in ensemble data and can access unidirectional rate constants for reversible reactions. Many SM enzyme turnover studies have involved H-transfer chemistry to intrinsic cofactors.[16−19] Despite the power of SMS, the relatively low intrinsic fluorescence of natural cofactors has limited widespread adoption of SMS to study enzyme turnover. spFRET can overcome this limitation.[17,20−22] In spFRET, the high fluorescence emission of an extrinsic label (a so-called 'molecular beacon') attached to the target enzyme is modulated by redox cycling of the enzyme cofactor through FRET. Uniquely, SM KIE measurements are used to deconvolve chemical and other dynamical contributions to SM fluorescence time traces, a problem that is inherent to SM turnover studies. These studies were performed using pentaerythritol tetranitrate reductase (PETNR), a redox enzyme that contains a single flavin mononucleotide (FMN) redox cofactor. This cofactor is alternatively reduced and oxidized in two half-reactions involving hydride transfer from the *pro*-R hydrogen of coenzyme NADH, then oxidation by molecular oxygen (Figure 1A) or an oxidative substrate such as pentaerythritol tetranitrate. Ensemble-based KIE measurements have indicated that the hydride transfer from NADH to FMN catalyzed by PETNR involves quantum mechanical tunneling (QMT).[10,23] Oxidised FMN is highly fluorescent in solution, but the emission is quenched appreciably (~100-fold) when bound to PETNR. spFRET was used to enhance the SM fluorescence signal to record time traces of FMN reduction and oxidation during catalysis with NADH and the deuterated counterpart (*R*)-[4-^{2}H]-NADH (Figure 1A). We report SM analysis of reaction rates for this hydride transfer reaction. We demonstrate how KIE values can be extracted from SM reaction data and used to inform on the contributions of nonenzymatic dynamics and reaction chemistry to SM fluorescence data.

Received: September 19, 2012
Published: February 12, 2013

   dx.doi.org/10.1021/ja309286r | *J. Am. Chem. Soc.* 2013, 135, 3855−3864

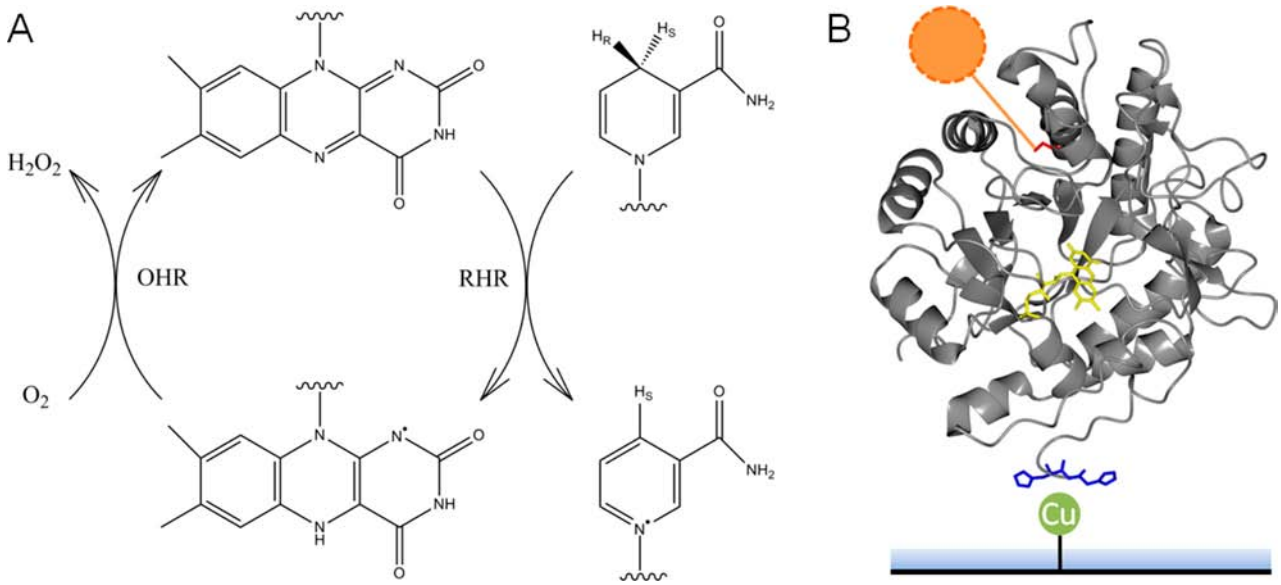

Figure 1. (A) PETNR catalytic cycle. In the reductive half reaction, hydride transfer proceeds from the C4 *pro-R* hydrogen of NADH to the N5 atom of FMN. The oxidative half reaction may proceed with molecular oxygen, giving H_2O_2, though the precise mechanism is poorly understood. (B) Experimental setup to monitor PETNR FMN redox state by SM TIRF microscopy. Laser excitation gives rise to total internal reflection of the excitation beam. Alexa-488 (orange sphere) attached to a PETNR molecule immobilized on the surface is excited by the evanescent field and undergoes FRET to the FMN. Emission of the Alexa-488 moiety is monitored.

RESULTS

SM Detection of PETNR by Total Internal Reflection Fluorescence (TIRF) Microscopy. Enzyme turnover and motion was monitored under SM conditions using TIRF. Supporting Information Figure S1 shows the TIRF experimental setup. The detailed setup and methods for data extraction and processing are explained in more detail in Methods. Briefly, PETNR was labeled with an extrinsic fluorophore (Alexa-488) attached by a maleimide linkage to the only native cysteine residue (Cys-222). PETNR-Alexa-488 was then immobilized on a copper-functionalized coverslip through a poly histidine tail engineered to extend the natural C-terminus of PETNR (Figure 1B).[24] The immobilized enzyme was excited at 488 nm under TIRF conditions and fluorescence emission from the extrinsic fluorophore was monitored temporally with a 12 ms time resolution. A typical example of fluorescence emission from a SM of labeled PETNR in the absence of NADH is shown in Figure 2A. Alexa-488 emission is stable for several seconds, typically photobleaching after ~5 s. While photobleaching is suppressed by oxygen removal, oxygen is required for SM enzyme turnover, where it acts as the oxidant during the oxidative half-reaction (Figure 1A).

SM Dynamics of PETNR-Alexa-488. Fluorophores at the SM level typically show stochastic fluctuation between different emission states. When attached to proteins, this fluctuation has been attributed to transient interaction of the fluorophore with aromatic residues[25,26] or artificial quenchers,[19] giving rise to either quenching or enhancement of fluorescence emission. Fluctuations were observed in the fluorescence time traces of PETNR-Alexa-488 (Figure 2A), possibly reflecting alternate protein−fluorophore conformations (fluorophore-specific contributions to the emission fluctuation are also possible; see Supporting Information for details). Noise will be a contributing factor to the observed SM signal. However, the aim is to characterize the SM signal from PETNR-Alexa-488 prior to turnover studies, rather than investigate the specific contributions to the PETNR-Alexa-488 signal. A total of 70 PETNR-Alexa-488 SMs and their associated emission transitions (350 transitions) were monitored, from which frequency data were derived. SM frequency data for dwell times between fluorescence states, $f(\tau)$, are typically analyzed by fitting to exponential decay functions.[27] Figure 2B shows binned τ values for PETNR-Alexa-488 fit to a single exponential decay (implying a single population) giving an apparent rate for transition between different emission states of $k_{app} = 4.0 \pm 0.1$ s^{-1}. However, fitting dwell time data in this way can mask more complicated kinetics as similar apparent rates will not be resolved readily using exponential functions. Consequently, we plotted the frequency of the apparent rate, $f(k)$ (where $k = 1/\tau$), which appears to be approximately Gaussian on a $\log_{10}$ scale (Figure 2C).[28] This approach has been used in previous SM studies but, we note, represents an approximation.[29] A range of other fitting approaches have been used for these type of data, though we found in practice fitting Gaussians to our log k data was the most robust method of extracting multiple populations from frequency data, though we emphasize that this should only be used to extract the midpoint of log k frequency data. From Figure 2C, it is apparent that there are actually two well-defined populations, fitting to a multi-Gaussian function (eq 1) comprising two species. This multicomponent data set is mirrored in the frequency data for the emission intensities, $f(\Delta Em)$, reflecting interchange between each emission state (Figure 2D). The fitted data suggest the presence of a major species [$f(\log k) = 86\%$ and $f(\Delta Em) = 81\%$ of the integrated area] and a minor species [$f(\log k) = 14\%$ and $f(\Delta Em) = 19\%$ of the integrated area], shown as red (major) and blue (minor) dashed lines in Figure 2C,D. However, there is no significant correlation between the magnitude of the ΔEm and log k values. The major species exhibits a 'slow' apparent rate for interconversion with a midpoint of 3.4 ± 0.1 s^{-1} (Figure 2C) centered about the average relative emission intensity ($\langle \Delta EM \rangle = 0$) with a value of -0.02 ± 0.01 (Figure 2D). The minor species exhibits an apparent interconversion rate of 8.0 ± 0.1

dx.doi.org/10.1021/ja309286r | J. Am. Chem. Soc. 2013, 135, 3855−3864

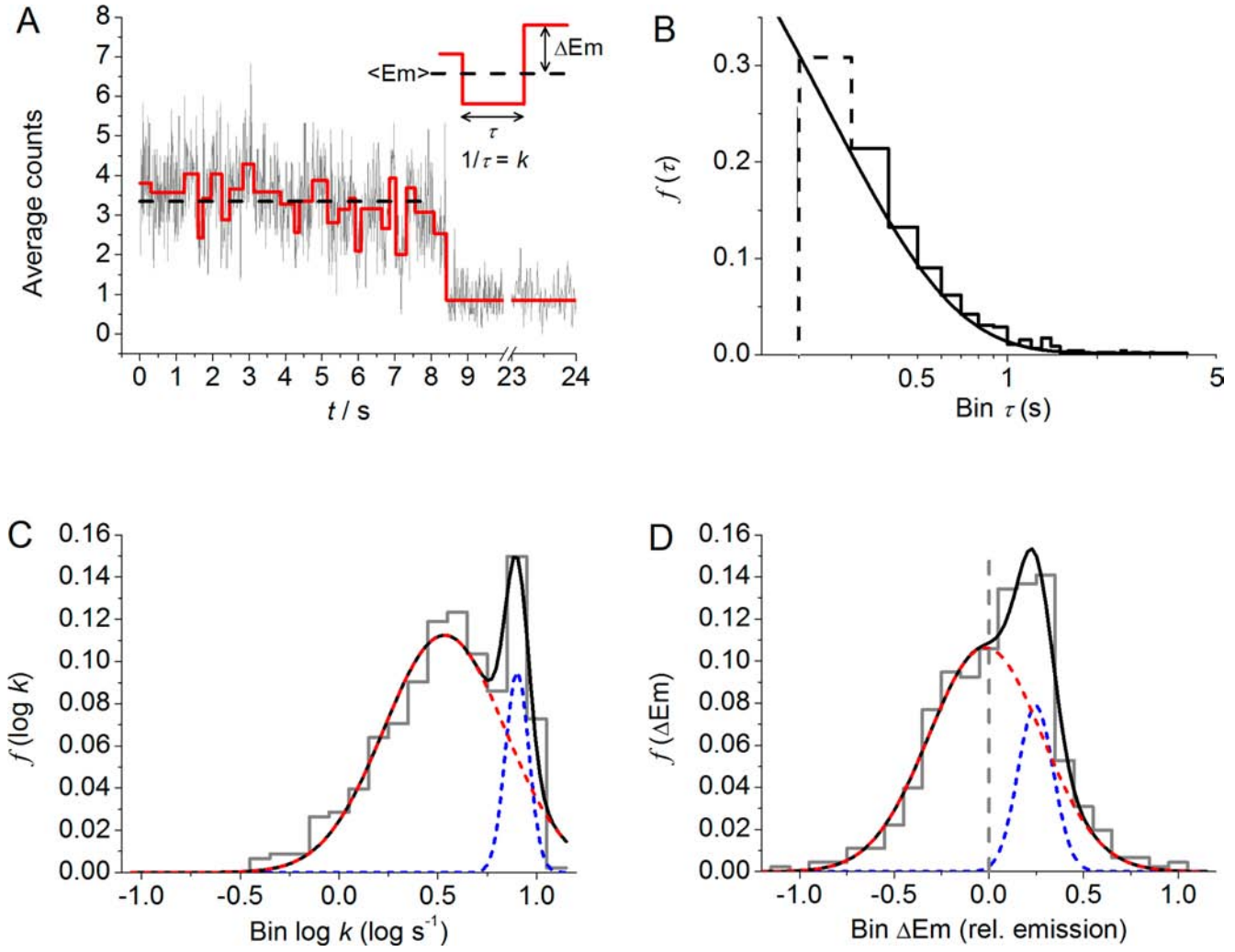

Figure 2. (A) Fluorescence intensity fluctuation of a single labeled PETNR molecule. The red line shows the fit to an edge finding algorithm (see Supporting Information for details) that identifies transitions between fluorescence states and the dashed gray line shows the average emission of the nonphotobleached region. The inset shows how the values of k and ΔEm are extracted, where $k = 1/\tau$, and τ is the dwell time and ΔEm = Em − ⟨Em⟩, and ⟨Em⟩ is the average fluorescence intensity. Combining and binning ∼500 of these extracted k and ΔEm values gives rise to frequency distributions extracted from enzyme-only single molecule time series for (B) $f(\tau)$, (C) f(log k) and (D) f(ΔEm). The black line in (B) is the fit to a single exponential decay function. The dashed section represents an oversampled region of the data at very small τ values and for this reason is not included in the fitting. The black line in (C) and (D) is the fit to a multi-Gaussian function (eq 1) with two components shown as red and blue dashed lines.

s^{-1} (Figure 2C) centered at a significantly larger than average relative emission intensity of 0.25 ± 0.01 (Figure 2D). The observation of asymmetric frequency data for both f(log k) and f(ΔEm) suggest that noise alone cannot account for the observed SM signal. Although the origin of these two components was not investigated, Alexa-488 has been shown previously to exist in two environments when bound to protein.[30] It is important to note that, based on the X-ray crystal structure of PETNR, the distance between the FMN and Alexa-488 moieties is expected to be ∼30 Å. This compares to a Förster radius, R_0, of 36 Å calculated for the FMN/Alexa-488 FRET pair (Supporting Information Figure S2). Consequently, the SM spFRET efficiency is expected to be highly sensitive to fluctuation of both the FMN and Alexa-488 moieties. In SM studies of enzyme catalysis (vide infra), it will be necessary to deconvolute these background signals from spFRET signals that report on changes in redox state of the active site FMN attributed to enzyme turnover.

SM Turnover of PETNR-Alexa-488. Prior to SM turnover experiments, PETNR-Alexa-488 was used in ensemble stopped-flow studies to enable comparison with unmodified PETNR (Figure 3A,B). The fluorescence emission of Alexa-488 was monitored following rapid mixing of PETNR-Alexa-488 with saturating NADH in a stopped-flow instrument. Monitoring of Alexa-488 emission enabled comparison of the spFRET kinetic parameters of PETNR-Alexa-488 with those for reduction of PETNR acquired by absorption (FMN reduction) stopped-flow spectroscopy (Figure 3A). A KIE of 6.8 ± 0.4 (PETNR-Alexa-488) is similar to the reported KIE of 8.1 ± 0.1 (PETNR) and observed rate constants for flavin reduction are also similar (Figure 3B).[10] Further, the temperature dependence of the KIE ($\Delta\Delta H^{\ddagger}$) for PETNR-Alexa-488 (1.6 ± 2.3 kJ mol^{-1}) is similar to that for PETNR (−1.1 ± 2.1 kJ mol^{-1}). These ensemble studies indicate that the kinetic properties of PETNR-Alexa-488 (monitoring both fluorescence from Alexa-488 and also FMN absorption changes) are similar to those published for PETNR with NADH as reducing coenzyme.

dx.doi.org/10.1021/ja309286r | J. Am. Chem. Soc. 2013, 135, 3855−3864

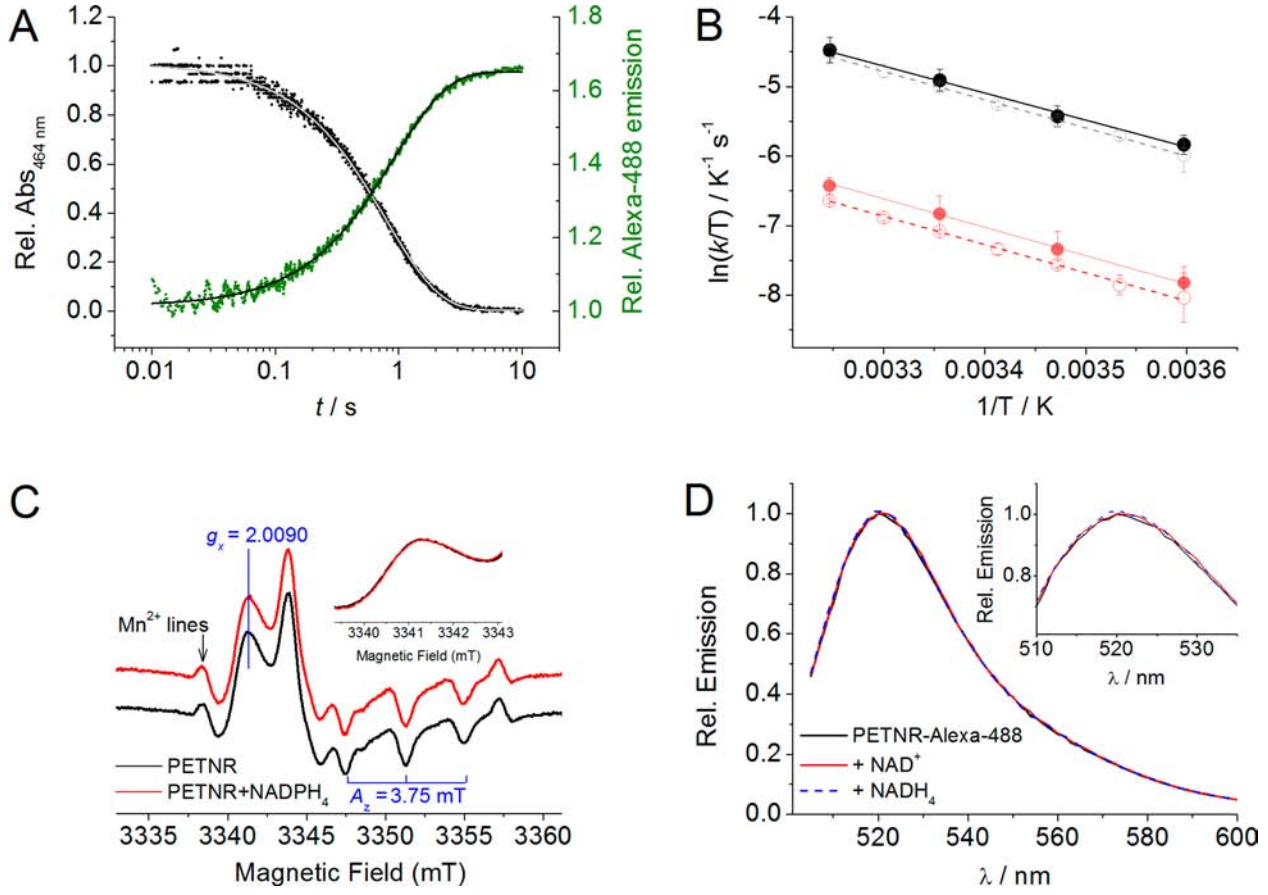

Figure 3. The effect of an extrinsic label on PETNR activity. (A) Example stopped-flow transients of PETNR-Alexa-488 show the exponential decay of flavin absorbance (black) corresponds with the rise of Alexa-488 emission (green) at 15 °C. Data are fit to a single exponential function (gray line), giving similar observed rate constants and activation energies. Conditions: 50 mM potassium phosphate pH 7, 25 mM coenzyme and ~0.5 μM PETNR-Alexa-488 excited at 490 nm, with emission measured using a 550 nm cutoff filter or absorbance monitored at 464 nm. (B) Temperature-dependence of the observed rate of FMN reduction for both PETNR (open circles; determined previously[2]) and PETNR-Alexa-488 (closed circles) with NADH (black) or (*R*)-[4-^{2}H]-NADH (red). Solid lines show fits to the Eyring equation. (C) 94-GHz continuous-wave EPR spectra of PETNR (black line) in the presence of the nonreactive coenzyme mimic, $NADPH_4$ (red line) in 50 mM potassium phosphate, pH 7. Spectra were recorded at 120 K, modulation amplitude = 0.8 mT, 0.0048 mW, 100 kHz, 16 scans. The features with a spacing of ~9 mT are Mn^{2+} hyperfine lines arising from cavity background. Inset shows expansion of g_x region. (D) Coenzyme binding does not alter extrinsic fluorophore emission. Incubation of PETNR-A488 with the coenzyme mimics NAD^+ and 1,4,5,6-tetrahydro-NADH ($NADH_4$) (5 mM) give no observable change in Alexa-488 emission spectrum, suggesting coenzyme binding does not contribute to the observed SM signal. Conditions: 50 mM potassium phosphate pH 7, 5 mM coenzyme and ~0.5 μM PETNR-A488 excited at 490 nm.

Therefore, Alexa-488 does not compromise the H-transfer chemistry of PETNR and the observed rate constant for FMN reduction are accurately recapitulated using the spFRET method.

We have also investigated the effect of coenzyme binding on the conformation of an extrinsic label in PETNR to assess if coenzyme binding induces conformational change at the site of the extrinsic label. We have monitored high-field (94-GHz) electron paramagnetic resonance (EPR) spectra of a nitroxide spin label, bound to PETNR at the same position as Alexa-488 (Figure 3C). We find that the g_x and A_z values are essentially identical between coenzyme ($NADPH_4$) bound and free forms of PETNR. These parameters reflect features of the local surrounding such as polarity.[31] The EPR data therefore suggest that there is not a large scale conformational change upon coenzyme binding that will perturb an extrinsic label. Indeed, we find that the emission of Alexa-488 is invariant with either NAD^+ or the nonreactive coenzyme mimic, $NADH_4$ bound (Figure 3D).

SM turnover of PETNR was monitored as fluctuations in fluorescence time traces in the presence of NADH and oxygen. These fluorescence time traces include contributions from low fluorescence 'off' (oxidized FMN) and high fluorescence 'on' states (reduced FMN) as well as redox independent fluorescence changes attributed to motions of the probe, cofactor and/or enzyme (vide supra) (Figure 4A). The two redox states encompass the complete catalytic cycle comprising the two half-reactions (Figure 1A). Given current interest in H-transfer reactions, the focus here is on the reductive half-reaction (FMN reduction by NADH); the oxidative half-reaction (FMN oxidation by molecular oxygen) is shown in Figure 5 and discussed in Supporting Information (Figures S6 and S7).

Approximately 100 PETNR-Alexa-488 SMs and their associated emission transitions [for FMN reduction: 446, NADH; 430, equimolar NADH/(*R*)-[4-^{2}H]-NADH; and 502, (*R*)-[4-^{2}H]-NADH] were monitored, from which frequency data were derived. The frequency of dwell times with NADH (Figure 4B; blue line) was fitted to a single exponential decay

dx.doi.org/10.1021/ja309286r | J. Am. Chem. Soc. 2013, 135, 3855−3864

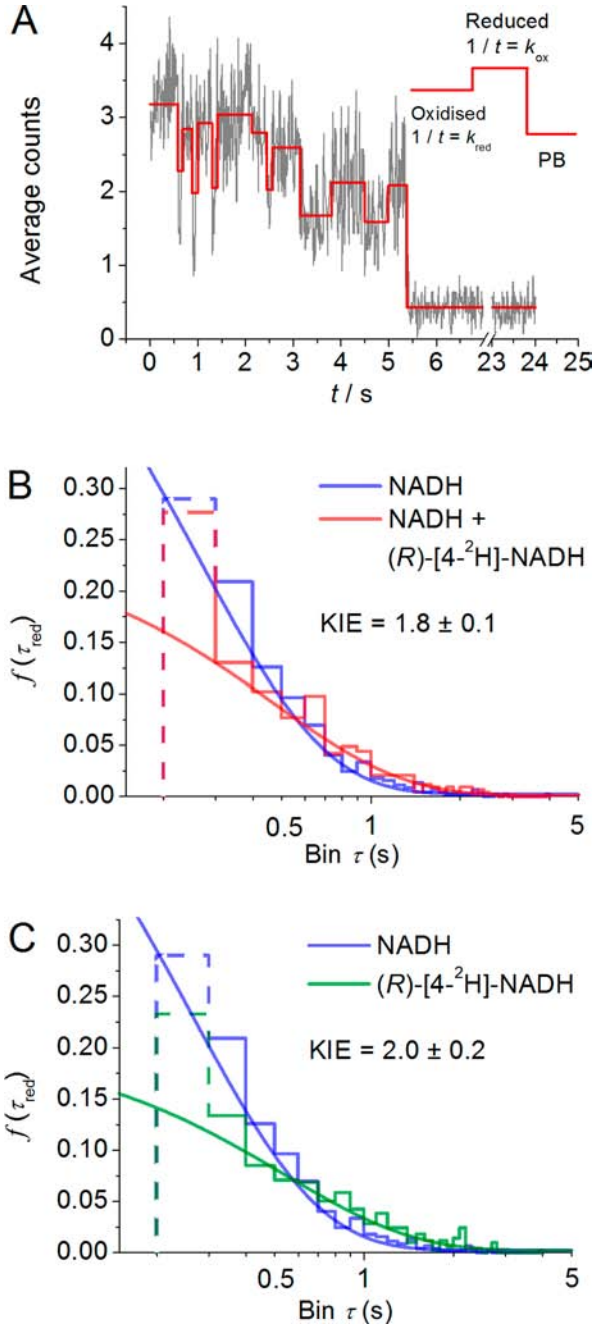

Figure 4. (A) Example SM track showing FMN turnover by monitoring Alexa-488 emission. In an idealized case, three distinct fluorescence emission states of Alexa-488 can be monitored attributable to reduced FMN (high emission), oxidized FMN (low emission) and photobleached (PB). The frequency data extracted from the SM time series for $f(\tau)$ with NADH, equimolar NADH + (*R*)-[4-^{2}H]-NADH (B), and (*R*)-[4-^{2}H]-NADH (C). The solid lines are the fit to a single exponential decay function. Fitting to additional exponential components did not significantly improve the fitting statistics. The dashed section represents oversampled regions of the data which are not included in the fitting.

function as with PETNR-Alexa-488 alone (Figure 3B). The apparent rate (k_H = 3.8 ± 0.1 s^{-1}) is similar to that for PETNR-Alexa-488 in absence of NADH (k_{app} = 4.0 ± 0.1 s^{-1}). However, as discussed above, this analysis is likely to mask complexity in the data. Analyzing the data in this way suggests that there is no observable chemical turnover with NADH, but more likely is that the rate of FMN reduction coincides with the signal attributed to PETNR-Alexa-488 alone. To improve the ability of SM detection to extract chemistry from system specific dynamics/noise, we turned to KIE measurements. A significant KIE is manifest where a kinetic probe is able to resolve a hydrogen transfer step. Stereospecific deuteration at the primary (*pro* R) position of NADH gives rise to a decrease in the observed rate constant for hydride transfer.[10] This gives access to the primary KIE at the SM level. Isotopic substitution is not thought to alter the reactive complex geometry, so the SM data from both NADH and (*R*)-[4-^{2}H]-NADH should report on directly comparable SM states. To extract the SM KIE, we titrated increasing concentrations of the deuterium-labeled coenzyme NADH isotopologue (*R*)-[4-^{2}H]-NADH and extracted SM frequency data (Figure 4B,C). Fitting the resulting frequency data $f(\tau)$ to a single exponential component gives significantly lower apparent rate of FMN reduction for an equimolar mixture of NADH and (*R*)-[4-^{2}H]-NADH (Figure 4B) and (*R*)-[4-^{2}H]-NADH alone (Figure 4C), k_D = 2.1 ± 0.1 s^{-1} and k_D = 1.9 ± 0.2 s^{-1}, respectively. These data demonstrate that there is a shift to lower observed rates of FMN reduction upon isotopic substitution and that the effect is concentration dependent, with the apparent KIE increasing with increasing (*R*)-[4-^{2}H]-NADH. That said, these data are complex and fitting to a single exponential function is clearly a gross oversimplification, particularly where two substrates are used together.

As with PETNR-Alexa-488 alone, the frequency data for the apparent rates [f(log k)] of formation of the reduced form of the enzyme is complex (Figure 5A−C). The distribution is described by a multi-Gaussian function (eq 1) with at least two components: $n \geq 2$ in eq 1 (Figure 4C). With NADH there is no significant difference between the PETNR-Alexa-488 and PETNR-Alexa-488 + NADH log k data (P_1 = 0.12, Methods and Supporting Information for details). However, an analysis of the frequency data for fluorescence states, $f(\Delta Em)$, with both NADH and (*R*)-[4-^{2}H]-NADH (Supporting Information Figure S3 and Table S1), suggests that additional (n > 2) Gaussian components are required to adequately fit the SM turnover data as described in Supporting Information. The log k frequency data for FMN reduction with (*R*)-[4-^{2}H]-NADH (Figure 5B and C) is different from that for NADH (Supporting Information Figure S4), with the log k data showing a significant difference to the PETNR-Alexa-488 only control (P_1 < 0.0001). Indeed, a multi-Gaussian fitting function (eq 1) with three components is required to adequately fit both equimolar NADH/(*R*)-[4-^{2}H]-NADH and (*R*)-[4-^{2}H]-NADH alone log k_{red} frequency data (Figure 5B,C).

On the basis of SM studies with PETNR-Alexa-488 alone, the component of the frequency data attributed to states unrelated to turnover can be simulated using the fitting parameters extracted from Figure 2C (Figure 5A−C, black dashed line). This enabled extraction of the frequency data due to FMN reduction as a third Gaussian component (Figure 5A−C, colored line). The apparent rate extracted from the midpoint of the third Gaussian component with NADH (k_{red} = 4.1 ± 3.3 s^{-1}), equimolar NADH/(*R*)-[4-^{2}H]-NADH (k_{red} = 1.84 ± 3.1 s^{-1}), and (*R*)-[4-^{2}H]-NADH alone (k_{red} = 1.1 ± 0.9 s^{-1}). These values compare favorably with observed rate constants for this reaction determined from ensemble stopped-flow studies.

As the fraction of (*R*)-[4-^{2}H]-NADH is increased, there is a trend to increasingly slow rates and therefore larger KIEs: with equimolar NADH/(*R*)-[4-^{2}H]-NADH, midpoint KIE = 2.7 ±

dx.doi.org/10.1021/ja309286r | J. Am. Chem. Soc. 2013, 135, 3855−3864

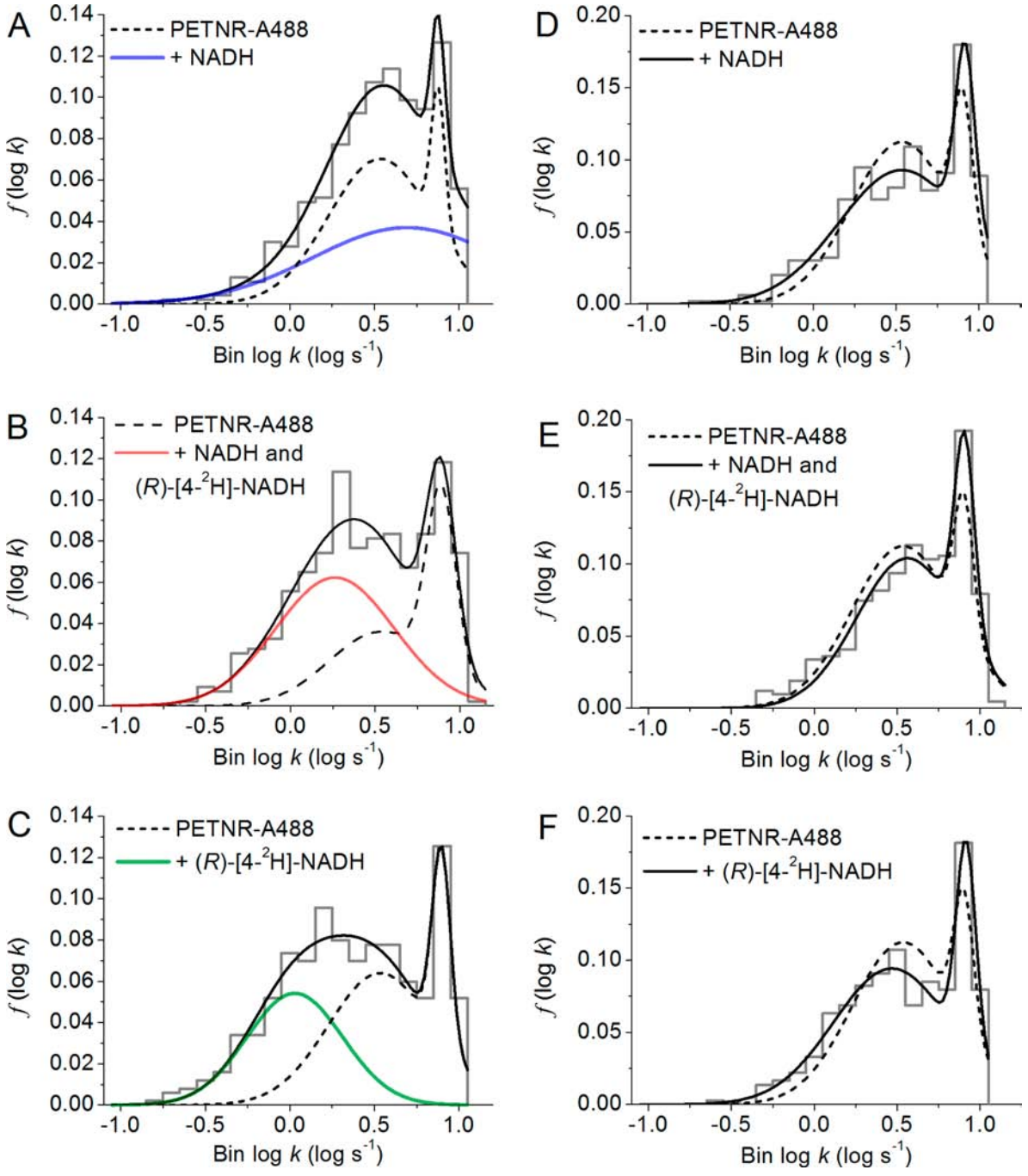

Figure 5. The frequency data extracted from the SM time series for $f(\log k)$ for reduction (A–C) and oxidation (D–F) of PETNR in the presence of NADH (A and D), equimolar NADH and (*R*)-[4-^{2}H]-NADH (B and E), and (*R*)-[4-^{2}H]-NADH (C and F). In panels A–C (FMN reduction), the black fitted line is a convolution of three Gaussian components, two described by the black dashed line and one described by the colored line. The dashed gray line shows the simulation of the frequency data attributable to protein motion extracted from Figure 2C; note that only the width and midpoint of the two Gaussians are fixed, the area of each of the components is allowed to vary in the fitting. The colored line is then the fit to the frequency data that is attributable to FMN reduction with either NADH (blue), a mixture of NADH and (*R*)-[4-^{2}H]-NADH (red), or (*R*)-[4-^{2}H]-NADH alone (green). In panels D–F (FMN oxidation), the black fitted line is a convolution of two Gaussian components, fitted to the SM frequency data. The dashed line shows the fit to the PETNR-Alexa-488 only data and corresponds to the fitted line in Figure 2C but the area of each Gaussian component is allowed to vary as described in Methods.

4.7 and with (*R*)-[4-^{2}H]-NADH alone, midpoint KIE = 3.7 ± 4.2. The SM FMN reduction data (Figure 5B,C) are contrasted by the SM FMN oxidation data (Figure 5D,E). There is no significant difference between the SM FMN oxidation frequency data and the enzyme only log *k* data as shown by the similarity of the PETNR-Alexa-488 Gaussian fits (dashed line; Figure 5D,E) and SM FMN oxidation frequency data fit to a two Gaussian function (solid line, Figure 5D,E). FMN oxidation is slow (<0.2 s^{-1}), and therefore largely outside of the detectable range of our SM experiments. The SM FMN oxidation data therefore act a control for the effect of increasing (*R*)-[4-^{2}H]-NADH concentration, demonstrating that the observed KIE is attributable solely to FMN reduction. An increase in the SM midpoint KIE as a function of increasing

dx.doi.org/10.1021/ja309286r | J. Am. Chem. Soc. 2013, 135, 3855–3864

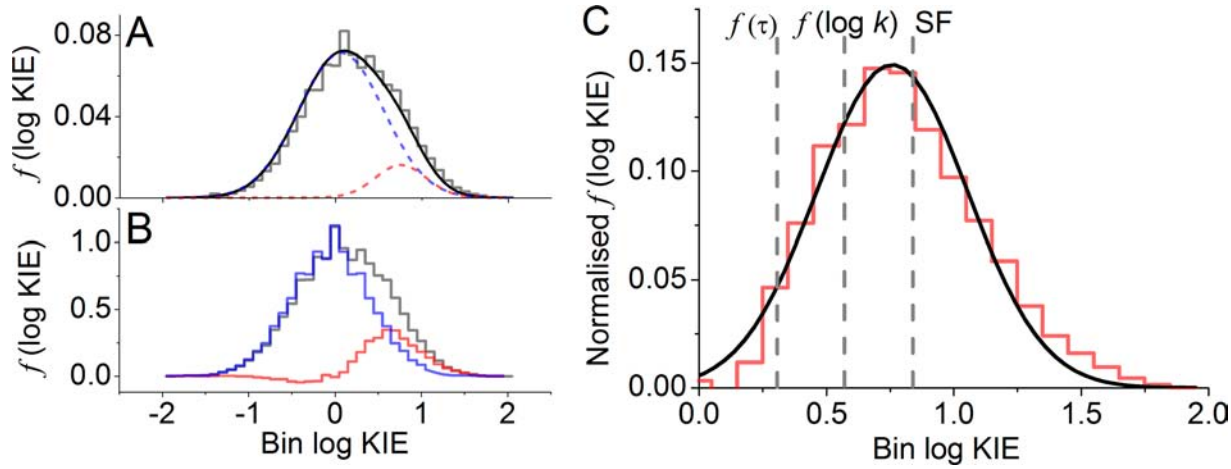

Figure 6. (A) The unbinned SM frequency-domain data can be combined to form all possible pairwise KIE values to give the frequency data of KIEs (gray stepped line). These data can be fit with two-Gaussian components shown as the black fitted line, comprising the data shown by the dashed blue line and the dashed red line. (B) Alternatively, we deconvolve the processes that do not reflect FMN reduction ($\log_{10}$ KIE = 0) in a model free manner by subtracting the KIE values determined for turnover with NADH alone (blue stepped line). The resulting frequency data (red stepped line) has a small negative component arising from overlap of the NADH and (*R*)-[4-^{2}H]-NADH values. (C) Comparison of the SM KIE values extracted using the various methods described in the main text. The model free KIE frequency data determined from the KIE data in Figure 5C is now shown as a black line (red dashed line in Figure 5A) and as a red stepped line (red stepped line in Figure 5B). Dashed vertical lines indicate the values extracted for ensemble stopped-flow data (SF), the midpoint KIE from the SM log *k* data shown in Figure 5A,C [f(log *k*)] and the KIE extracted from the dwell time data shown in Figure 4B [$f(\tau)$].

isotopologue concentration is therefore very clear evidence that SM FMN reduction with NADH is hidden in the enzyme only signal and that we are able to deconvolve reaction chemistry from other factors such as intrinsic dye dynamics and signal noise using the SM KIE approach. Moreover, fitting Gaussian components to log *k* frequency data provides a significant improvement in the accuracy of the extracted KIE giving a more comparable value to the ensemble KIE. We note, however, that the fitting of the log *k* frequency data is complex. Therefore, we next explored the use of model free methods to extract the SM KIE.

Extracting the SM KIE. The SM KIE value was extracted from the unbinned apparent SM rate constant (frequency-domain) using a model free method (Figure 6A; gray stepped line) described in Methods. A detailed discussion and validation of the model free method is provided in Supporting Information. On a $\log_{10}$ KIE scale, these bins can also be fit to a multi-Gaussian function comprising two species (Figure 6A, black line). Unlike log *k* data, the binned log KIE data should be symmetrical and therefore accurately fit by a function such as a Gaussian (see Supporting Information Figure S7). These data fit with a major species (88% by area) with a midpoint KIE of 1.2 ± 0.5 and a minor species (12% by area) with a midpoint KIE of 5.7 ± 0.3. Since the KIE is specifically sensitive to FMN reduction, we expect a large proportion of the unbinned time domain data to give a KIE of essentially unity, reflecting the apparent rates for intrinsic, nonenzymatic processes. The Gaussian component showing a KIE > 1 is then attributable to FMN reduction. As an alternative, we have extracted all combinations of KIE values for turnover with NADH alone (Figure 6B; blue stepped line) and subtracted these data from that calculated for both NADH and (*R*)-[4-^{2}H]-NADH (Figure 6B; gray stepped line). These new data (Figure 6B; red stepped line) reflect KIE values attributable to FMN reduction alone, deconvolved from enzyme/dye motion and other processes which do not reflect FMN reduction. Crucially, this is a model free method of extracting the KIE and does not assume that the binned rate and/or KIE values are normally distributed over log *k* or KIE, respectively. This method yields a major species (79% by area) with a midpoint KIE of 1.0 and a minor species (21% by area) with a midpoint KIE of 4.7.

DISCUSSION

Deconvolving Chemistry from Other SM Signals. In the SM enzyme catalysis field, it has been typical to plot the binned dwell time of SM enzyme turnover data and fit these to an exponential decay function to extract an apparent rate constant for the mechanistic step of interest.[16,19,32,33] However, as shown here, plotting SM apparent rate ($k_{app} = 1/\tau$) data on a log scale exposes a multicomponent data set with similar apparent rates. This highlights a major advantage of using SM methods (vs ensemble methods) to analyze these types of reactions: multiexponential functions struggle to deconvolve multicomponent time-domain data with similar rates. This is clearly the case with SM data reported here, where a multiexponential function does not resolve the identified multiple populations. We thus caution against use of exponential fitting functions in SM studies of enzyme turnover as this might lead to erroneous conclusions about the presence and assignment of observed SM populations (vide infra).

Gaussian fitting of SM log *k* data for PETNR-Alexa-488 (in absence of NADH) suggests there is interconversion between major and minor states. The simplest model implies the major species reflect a conformation for PETNR-Alexa-488 in which the dye is quenched. The minor species reflects a distinct conformational state in which the Alexa-488 dye is less quenched.[30] Extracting these multiple components is required for subsequent determination of apparent rates for FMN reduction. This should be a general approach in studies of SM enzyme catalysis where processes involving the introduced probe, active site cofactor or protein could in principle (or in all likelihood) complicate SM fluorescence time traces.

dx.doi.org/10.1021/ja309286r | J. Am. Chem. Soc. 2013, 135, 3855−3864

SM analysis of the 'resting' form of PETNR-Alexa-488 alongside turnover studies with NADH and oxygen identified a new component that we attribute to FMN reduction. The apparent rates for SM FMN reduction are broadly consistent with previous SM studies of enzyme turnover,[16,18,34] showing a broad range of rates spanning several orders of magnitude. This variation in apparent rate is often attributed to microscopic structural heterogeneity in the enzyme reactive complex and/or to the existence of multiple chemical barriers to reaction, which represent a complex free energy landscape for enzyme catalysis.[16,18,35] The present study is in general agreement with previous SM enzyme turnover measurements with respect to the overall distributed range of apparent rates. However, our studies highlight the need to account for any background signals and/or broadening attributable to both intrinsic and extrinsic cofactors as well as noise. Interpreting the width of SM frequency data remains a key challenge when analyzing SM data sets; a rigorous quantitative dissection of the contributing factors, which includes the inherent instrumental noise, is challenging.[36]

Single Molecule Kinetic Isotope Effects. KIEs at the SM level have been observed rarely in nonbiological/biological systems involving the reaction of a quinone and thiol within an artificial pore structure[37] and in turnover of DHFR.[38] As we discuss below, access to SM enzymatic KIEs will provide new information on enzymatic H-transfer reactions and so the development of robust methods to measure SM KIEs is essential. In the work reported here, SM KIEs were extracted in several ways. The KIE extracted from exponential decay functions fitted to the dwell time data (Figure 4C) gives a KIE of 2.0 ± 0.2. This value is significantly smaller than measured by the corresponding ensemble method with PETNR-Alexa-488 (KIE = 6.8 ± 0.4). The KIE extracted from the midpoints of Gaussian fits with NADH (Figure 5A) and (*R*)-[4-^{2}H]-NADH (Figure 5C) is 3.7 ± 4.2. This KIE value is closer to that observed in stopped-flow ensemble studies of PETNR reduction, though the error is large.

A potentially more robust way of extracting the SM KIE value is shown in Figure 5A,B, based on extracting the KIE from all combinations of SM apparent rates (see Methods). The KIEs for FMN reduction [KIE = 5.7 ± 0.3 (Figure 6A; Gaussian fitting method) or 4.7 ± 0.2 (Figure 6B; model free method)] are comparable with values determined at the ensemble level (KIE = 6.8 ± 0.4) as shown in Figure 6C. Extracting the KIE in this way gives a closer value to the ensemble KIE and a more reasonable error compared to using the midpoints of the Gaussians attributable to NADH and (*R*)-[4-^{2}H]-NADH (KIE = 3.7 ± 4.2) as shown in Figure 6C. These more accurate values derived from extracting a matrix of KIE values likely reflects the more appropriate fitting of KIE data to a Gaussian function compared to log(*k*) frequency data (Supporting Information Figure S7). A key finding is that we only find evidence for a single population of KIEs significantly larger than unity. Extracting the KIE in this way does not allow us to separate multiple populations with the same magnitude of KIE (e.g., that might arise from parallel reaction mechanisms). However, at the ensemble level, there is no evidence for alternative mechanistic pathways in PETNR and the chemical step (FMN reduction) is well-defined.[10,39]

***n*-State Models.** Recently '*n*-state' models have been proposed as an alternative explanation to distance sampling models of enzymatic H-tunnelling.[40] In *n*-state models, multiple reactive conformations are invoked to account for published ensemble data, specifically the temperature dependence of the KIE. The temperature dependence of KIEs has also been used to infer the presence of distance sampling in simple vibronic QMT models for H-transfer.[41−43] In the *n*-state model framework, at the SM level, a single discrete H-transfer population is expected where there is a corresponding temperature-independent KIE measured in ensemble studies. However, temperature-dependent KIEs at the ensemble level are expected to generate multiple populations at the SM level (assuming resolution of the populations is sufficient). Reduction of PETNR by NADH gives rise to a temperature-independent KIE at the ensemble level (Figure 3).[10] This is consistent with the single population of SM KIEs observed in Figure 5. These SM and ensemble data do not distinguish between *n*-state and distance sampling models, but studies with variant enzymes or the alternative coenzyme NADPH that give rise to ensemble temperature dependent KIEs would, in principle, distinguish between the two models. The principles and methods reported here for SM KIE measurements might therefore enable a rigorous test of the validity of the 'distance sampling' versus '*n*-state' model hypotheses.

■ CONCLUDING REMARKS

Here, we have monitored enzyme KIEs using SM approaches. Analysis of SM fluorescence time traces allows the contributions of nonenzymatic processes in the enzyme (or the label itself) to be deconvolved from those attributed to reaction chemistry. Using multiple methods to extract the SM KIE, we find that fitting exponential functions to SM dwell time data can significantly underestimate the complexity of SM data sets, and by extension the magnitude of the SM KIE. However, using a model free method for extracting the SM KIE gives very good agreement with ensemble data, providing excellent resolution of the intrinsic KIE. This approach provides a new experimental data set that may be used to benchmark QM/MM H-transfer calculations, which typically sample multiple MM snapshots and determine a range of apparent rates and KIEs.[44−46] SM KIEs enable analysis using physical models of catalysis not possible using ensemble-based data. This will present new opportunities for probing mechanisms of enzymatic H-transfer and the importance (or otherwise) of QMT, motions and multiple reactive states.

■ METHODS

Extrinsic Fluorophore Labeling of PETNR. PETNR-His$_8$ was expressed and purified as described.[24] Labeling of PETNR with the extrinsic fluorophore Alexa-488 was achieved by incubating PETNR in 50 mM potassium phosphate, pH 7 at <20 °C with 1 mM Alexa-488 C5-maleimide (Molecular Probes). Nonreacted fluorophore was separated from the sample by running through an Econ-Pac 10DG desalting column (Bio-Rad) equilibrated with 50 mM potassium phosphate, pH 7.

Ensemble Fluorescence and Absorbance Measurements. Fluorescence emission spectra were monitored on a Varian Cary Eclipse fluorescence spectrophotometer (Varian, Inc., Palo Alto, CA). Multiple wavelength absorbance spectra were monitored on a Varian Cary 50 Bio UV/vis spectrophotometer. All experiments were performed in 50 mM potassium phosphate, pH 7. To prevent oxidase activity of PETNR, all kinetic ensemble experiments were performed under strict anaerobic conditions within a glovebox (Belle Technology; <5 ppm O_2) using a Hi-Tech Scientific (TgK Scientific, Bradford on Avon, U.K.) stopped-flow spectrophotometer housed inside the glovebox. Spectral changes accompanying FMN reduction were monitored at 465 nm using a saturating concentration of NADH (5 mM) or (*R*)-[4-^{2}H]-NADH (5 mM), prepared as described

previously.[23] Fluorescence emission changes associated with FRET from Alexa-488 to FMN were monitored using a 550 nm short wave pass optical filter. Typically, 3−5 measurements were taken for each reaction condition. Reaction transients were fit using a single exponential function and the average rate constant ±1 standard deviation was used.

High-Field EPR. The 94-GHz continuous-wave EPR spectra were recorded using a Bruker E600 spectrometer equipped with a E600-1021H TeraFlex resonator and a liquid helium cryostat (Oxford Instruments). The field was calibrated against a separate sample of manganese/magnesium oxide (Mn(II)/MgO) standard. The absolute error in g-values was 1×10^{-4}.[47] EPR conditions are stated on the figure legend.

Objective-Type TIRF. A schematic of the experimental setup is shown in Supporting Information Figure S1. A 488 nm CW diode-pumped solid-state laser (Cyan-Scientific, Spectra Physics) of line width 1 MHz and M^2 = 1.1 was used for 488 nm excitation. The excitation beam was expanded by a factor of 10 to yield an approximately circular active FOV of diameter 56 μm at the sample. The laser was reflected from a dichroic mirror (505DCXR, Chroma) onto a high numerical aperture (NA) Nikon CFI Plan Apo 60 × 1.49 NA objective mounted on a Nikon TE300 inverted microscope. Optical contact between the sample slide and objective was made using fluorescence-free immersion oil, refractive index 1.518 (Zeiss, Immersol 518F). The fluorescence was collected by this same objective, passed through the dichroic and was imaged by an EMCCD camera (Evolve 512, Photometrics), after passing through further filters, as detailed in Supporting Information Figure S1 (DC2, 595DCXR; F1, 500-550 nm 525/50, Chroma).

Low density chelated copper coated 0.15 mm thick glass coverslips (Microsurfaces, Inc.) were mounted on a XY translation stage. Surfaces were verified to be free of fluorescent impurities. Highly dilute (50 pM) solutions of PETNR-A488 were drop-cast onto these surfaces, and immobilized via poly-His tag tethering. Fluorophore excitation was at 488 nm, using a power density of 150 mW/cm^2. Data acquisition was over 25 s with a data interval of 12 ms. For SM turnover measurements, a saturating concentration of NADH was used (5 mM). All experiments were performed in 50 mM potassium phosphate, pH 7.

Single Molecule Data Extraction and Analysis. Time-intensity trajectories of regions of interest (ROI) corresponding to single molecules were thresholded and extracted from the stacked raw data using a custom Visual Basic macro and image processing software (ImageProPlus v7.01). A simple 1D edge finding algorithm based on the method of Canny[48] downloaded freely as a Matlab (MathWorks) script from http://www.cs.unc.edu/~nanowork/cismm/download/edgedetector/index.html was used to extract the dwell times for oxidized and reduced states. Tracks were selected for analysis based on an absence of blinking events and emission longer than 5 s before photobleaching. This gives a minimum rate constant which can be extracted of 0.2 s^{-1} for every individual molecule analyzed. The edge fitting for each SM intensity track was thresholded until no edges were detected in the photobleached region. SM dwell times for FMN oxidation and reduction were extracted as continuous regions of high (increasing) or low (decreasing) fluorescence intensity until a transition to a lower or higher fluorescence state, respectively. The values of extracted rate constants (<10 s^{-1}) were significantly lower than the acqusition frame rate (~83 frames s^{-1}). Similar overall degrees of thresholding were used for PETNR-Alexa-488 alone and with each coenzyme, meaning there is no bias in the extracted dwell times from the data fitting. SM tracks extracted as either the average counts per pixel or as the maximum counts of the ROI gave equivalent fitting results. One tailed probabilities (P_1) are reported using the Mann−Whitney U test, where $P_1 < 0.05$ represents a significant difference between data sets.

The inverse dwell times for reduced states give the rate constants for FMN reduction. Histograms of the log rate constant, ΔEm and log KIE are fit to a multi-Gaussian function:

$$f(x) = \sum_{i=1}^{n}\left[\frac{A_i}{w_i\sqrt{\pi/2}}\exp\left(\frac{x-m_i}{w_i}\right)^2\right] \quad (1)$$

Where $f(x)$ is the frequency of a given value of $x = k$, ΔEm, or KIE (see below) given by the area, A, full width at half-maximal (fwhm), w, and midpoint, m of the Gaussian for the ith Gaussian component. The number of Gaussian components was determined by fitting increasing values of n, until the residuals of the fit ceased improving. To extract data from the fitting, we simultaneously fit 3 sets of the same data, binned at different intervals, sharing the constants for m and w, but not A as show in Supporting Information Figure S4. In this way, fitting bias due to bin interval selection is ameliorated.

To create the KIE data sets, each 'D' dwell time was divided by each 'H' dwell time. If there are i and j H and D dwell times, respectively, then this gives $i \times j$ KIE values. The $\log_{10}$(KIE) values were then binned. On a log KIE scale, these bins are symmetrical about log KIE = 0 if the same data are used for both the 'H' and 'D' data sets and otherwise are asymmetric (e.g., as in the case of the KIE calculation in Figure 6A; see also Supporting Information).

Abbreviations. TIRF, total internal reflection fluorescence; KIE, kinetic isotope effect; PETNR, pentaerythritol tetranitrate reductase; FRET, fluorescence resonance energy transfer; NADH, nicotinamide adenine dinucleotide; SM, single molecule; EPR, electron paramagnetic resonance.

■ ASSOCIATED CONTENT

Ⓢ Supporting Information

Supplement to the results and discussion, schematic of TIRF instrument, ensemble turnover and coenzyme binding studies and validation of data fitting. This material is available free of charge via the Internet at http://pubs.acs.org.

■ AUTHOR INFORMATION

Corresponding Author

nigel.scrutton@manchester.ac.uk

Present Address

†Christopher R. Pudney: University of Bath, Department of Biology and Biochemistry, Bath, BA2 7AY, UK.

Notes

The authors declare no competing financial interest.

■ ACKNOWLEDGMENTS

A. J. Fielding acknowledges a Bruker funded position. The work was funded by the UK Biotechnology and Biological Sciences Research Council (BBSRC) and Engineering and Physical Sciences Research Council (EPSRC). N.S.S. is a Royal Society Wolfson Merit Award holder and an EPSRC Established Career Fellow. S.H. is a BBSRC David Phillips Fellow.

■ REFERENCES

(1) Hogg, J. L.; Rodgers, J.; Kovach, I.; Schowen, R. L. *J. Am. Chem. Soc.* **1980**, *102*, 79.

(2) Kipp, D. R.; Hirschi, J. S.; Wakata, A.; Goldstein, H.; Schramm, V. L. *Proc. Natl. Acad. Sci. U.S.A.* **2012**, *109*, 6543.

(3) Roston, D.; Kohen, A. *Proc. Natl. Acad. Sci. U.S.A.* **2010**, *107*, 9572.

(4) Northrop, D. B. *Biochemistry* **1975**, 2644.

(5) Kohen, A. *Prog. React. Kinet. Mech.* **2003**, *28*, 119.

(6) Pudney, C. R.; Johannissen, L. O.; Sutcliffe, M. J.; Hay, S.; Scrutton, N. S. *J. Am. Chem. Soc.* **2010**, *132*, 11329.

(7) Meyer, M. P.; Tomchick, D. R.; Klinman, J. P. *Proc. Natl. Acad. Sci. U.S.A.* **2008**, *105*, 1146.

(8) Knapp, M. J.; Rickert, K.; Klinman, J. P. *J. Am. Chem. Soc.* **2002**, *124*, 3865.

(9) Loveridge, E. J.; Behiry, E. M.; Guo, J. N.; Allemann, R. K. *Nat. Chem.* **2012**, *4*, 292.
(10) Pudney, C. R.; Hay, S.; Levy, C.; Sutclife, M. J.; Leys, D.; Scrutton, N. S. *J. Am. Chem. Soc.* **2009**, *131*, 17072.
(11) Hothi, P.; Hay, S.; Roujeinikova, A.; Sutcliffe, M. J.; Lee, M.; Leys, D.; Cullis, P. M.; Scrutton, N. S. *ChemBioChem* **2008**, *9*, 2839.
(12) Heyes, D. J.; Sakuma, M.; Scrutton, N. S. *Angew. Chem .Int. Ed.* **2009**, *48*, 3850.
(13) Maglia, G.; Allemann, R. K. *J. Am. Chem. Soc.* **2003**, *125*, 13372.
(14) Kohen, A.; Klinman, J. P. *J. Am. Chem. Soc.* **2000**, *122*, 10738.
(15) Hay, S.; Sutcliffe, M. J.; Scrutton, N. S. *Proc. Natl. Acad. Sci. U.S.A.* **2007**, *104*, 507.
(16) Lu, H. P.; Xun, L. Y.; Xie, X. S. *Science* **1998**, *282*, 1877.
(17) Westphal, A. H.; Matorin, A.; Hink, M. A.; Borst, J. W.; van Berkel, W. J.; Visser, A. J. *J. Biol. Chem.* **2006**, *281*, 11074.
(18) Shi, J.; Dertouzos, J.; Gafni, A.; Steel, D.; Palfey, B. *Proc. Natl. Acad. Sci. U.S.A.* **2006**, *103*, 5775.
(19) Antikainen, N. M.; Smiley, R. D.; Benkovic, S. J.; Hammes, G. G. *Biochemistry* **2005**, *44*, 16835.
(20) Kuznetsova, S.; Zauner, G.; Aartsma, T. J.; Engelkamp, H.; Hatzakis, N.; Rowan, A. E.; Nolte, R. J.; Christianen, P. C.; Canters, G. W. *Proc. Natl. Acad. Sci. U.S.A.* **2008**, *105*, 3250.
(21) Goldsmith, R. H.; Tabares, L. C.; Kostrz, D.; Dennison, C.; Aartsma, T. J.; Canters, G. W.; Moerner, W. E. *Proc. Natl. Acad. Sci. U.S.A.* **2011**, *108*, 17269.
(22) Tabares, L. C.; Kostrz, D.; Elmalk, A.; Andreoni, A.; Dennison, C.; Aartsma, T. J.; Canters, G. W. *Chem. Eur. J.* **2011**, *17*, 12015.
(23) Pudney, C. R.; Hay, S.; Sutcliffe, M. J.; Scrutton, N. S. *J. Am. Chem. Soc.* **2006**, *128*, 14053.
(24) Toogood, H. S.; Fryszkowska, A.; Hulley, M.; Sakuma, M.; Mansell, D.; Stephens, G. M.; Gardiner, J. M.; Scrutton, N. S. *ChemBioChem* **2011**, *12*, 738.
(25) Choi, J.; Kim, S.; Tachikawa, T.; Fujitsuka, M.; Majima, T. *Phys. Chem. Chem. Phys.* **2011**, *13*, 5651.
(26) Neuweiler, H.; Banachewicz, W.; Fersht, A. R. *Proc. Natl. Acad. Sci. U.S.A.* **2010**, *107*, 22106.
(27) Flomenbom, O.; Velonia, K.; Loos, D.; Masuo, S.; Cotlet, M.; Engelborghs, Y.; Hofkens, J.; Rowan, A. E.; Nolte, R. J. M.; Van der Auweraer, M.; de Schryver, F. C.; Klafter, J. *Proc. Natl. Acad. Sci. U.S.A.* **2005**, *102*, 2368.
(28) McKinney, S. A.; Joo, C.; Ha, T. *Biophys. J.* **2006**, *91*, 1941.
(29) Sugawa, M.; Nishikawa, S.; Iwane, A. H.; Biju, V.; Yanagida, T. *Small* **2010**, *6*, 346.
(30) Rothwell, P. J.; Berger, S.; Kensch, O.; Felekyan, S.; Antonik, M.; Wöhrl, B. M.; Restle, T.; Goody, R. S.; Seidel, C. A. M. *Proc. Natl. Acad. Sci. U.S.A.* **2003**, *100*, 1655.
(31) Steinhoff, H. J.; Savitsky, A.; Wegener, C.; Pfeiffer, M.; Plato, M.; Möbius, K. *Biochim. Biophys. Acta* **2000**, *1457*, 253.
(32) Shi, J.; Palfey, B. A.; Dertouzos, J.; Jenson, K. F.; Gafni, A.; Steel, D. *J. Am. Chem. Soc.* **2004**, *126*, 6914.
(33) Guobin, L.; Wang, M.; Konigsberg, W. H.; Xie, X. S. *Proc. Natl. Acad. Sci. U.S.A.* **2007**, *104*, 12610.
(34) English, B. P.; Min, W.; van Oijen, A. M.; Lee, K. T.; Luo, G.; Sun, H.; Cherayil, B. J.; Kou, S. C.; Xie, X. S. *Nat. Chem. Biol.* **2006**, *2*, 87.
(35) Rissin, D. M.; Gorris, H. H.; Walt, D. R. *J. Am. Chem. Soc.* **2008**, *130*, 5349.
(36) Kalinin, S.; Sisamakis, E.; Magennis, S. W.; Felekyan, S.; Seidel, C. A. M. *J. Phys. Chem. B* **2010**, *114*, 6197.
(37) Lu, S.; Li, W. W.; Rotem, D.; Mikhailova, E.; Bayley, H. *Nat. Chem.* **2010**, *2*, 921.
(38) Zhang, Z.; Rajagopalan, P. T.; Selzer, T.; Benkovic, S. J.; Hammes, G. G. *Proc. Natl. Acad Sci. U.S.A.* **2004**, *101*, 2764.
(39) Pudney, C. R.; Hay, S.; Scrutton, N. S. *FEBS J.* **2009**, *276*, 4780.
(40) Glowacki, D. R.; Harvey, J. N.; Mulholland, A. J. *Nat. Chem.* **2012**, *4*, 169.
(41) Nagel, Z. D.; Klinman, J. P. *Nat. Chem. Biol.* **2009**, *5*, 543.
(42) Hay, S.; Scrutton, N. S. *Nat. Chem.* **2012**, *4*, 161.
(43) Kuznetsov, A. M.; Ulstrup, J. *Can. J. Chem.* **1999**, *77*, 1085.
(44) Pang, J. Y.; Hay, S.; Scrutton, N. S.; Sutcliffe, M. J. *J. Am. Chem. Soc.* **2008**, *130*, 7092.
(45) Hay, S.; Johannissen, L. O.; Sutcliffe, M. J.; Scrutton, N. S. *Biophys. J.* **2010**, *98*, 121.
(46) Pang, J. Y.; Pu, J.; Gao, J.; Truhlar, D. G.; Allemann, R. K. *J. Am. Chem. Soc.* **2006**, *128*, 8015.
(47) Burghaus, O.; Rohrer, M.; Gotzinger, T.; Plato, M.; Möbius, K. *Meas. Sci. Technol.* **1992**, *3*, 765.
(48) Canny, J. A. *IEEE Trans. Pattern Anal. Machine Intell.* **1986**, *8*, 679.